buildings

MDPI

Article

Experimental Study on Mechanical Properties and Drying Shrinkage Compensation of Solidified Ultra-Fine Dredged Sand Blocks Made with GGBS-Based Geopolymer

Ming Feng [1], Chaohua Jiang [1,*], Yixuan Wang [2], Yongqi Zou [1] and Junxian Zhao [1]

[1] College of Port, Coastal and Offshore Engineering, Hohai University, Nanjing 210098, China
[2] Faculty of Medicine, Nursing and Health Sciences, Monash University, Melbourne, VIC 3800, Australia
* Correspondence: chaohuajiang@hhu.edu.cn

Abstract: As natural aggregates become increasingly scarce, attention has turned to ultra-fine dredged sand (UDS) generated in waterway regulation engineering. UDS is typically challenging to utilize due to its high clay content and high water demand. This article uses ground granulated blast-furnace slag (GGBS)-based geopolymer to solidify UDS, along with sodium silicate (SS) and sodium hydroxide (SH) as alkaline activators. This paper explores the effects of SS modulus (SiO_2/Na_2O molar ratio) and mass percentage content of Na_2O on the fluidity, setting time, mechanical properties, and shrinkage behavior of hybrid UDS-GGBS geopolymer (HUGG) paste. According to the research findings, increased SS modulus and Na_2O content lead to decreased fluidity and setting time. When the Na_2O content reaches 6%, flash coagulation occurs in the slurry, leading to more internal shrinkage cracks and pores. This has been confirmed by scanning electron microscope (SEM) analysis. When Na_2O content is 5%, and SS modulus is 1.0, the 90-day maximum compressive strength reaches 56.53 MPa, corresponding to a splitting tensile strength of 6.83 MPa, which can be considered the optimal formulation. Meanwhile, basalt and polypropylene fibers (BF and PPF) are chosen to compensate for the susceptibility to drying shrinkage. Both BF and PPF can significantly inhibit the linear drying shrinkage of the HUGG paste. The BF's ability to enhance mechanical properties is more robust than PPF's, which can make the paste more homogeneous. The research contributes an effective method for the resource utilization of UDS.

Keywords: ultra-fine dredged sand; geopolymer; mechanical properties; microstructure; drying shrinkage

check for updates

Citation: Feng, M.; Jiang, C.; Wang, Y.; Zou, Y.; Zhao, J. Experimental Study on Mechanical Properties and Drying Shrinkage Compensation of Solidified Ultra-Fine Dredged Sand Blocks Made with GGBS-Based Geopolymer. *Buildings* **2023**, *13*, 1750. https://doi.org/10.3390/buildings13071750

Academic Editors: Fernando G. Branco and José Marcos Ortega

Received: 12 June 2023
Revised: 29 June 2023
Accepted: 8 July 2023
Published: 10 July 2023

Copyright: © 2023 by the authors. Licensee MDPI, Basel, Switzerland. This article is an open access article distributed under the terms and conditions of the Creative Commons Attribution (CC BY) license (https://creativecommons.org/licenses/by/4.0/).

1. Introduction

Waterway engineering projects, such as port construction and channel renovation, generate a significant amount of ultra-fine dredged sand (UDS), which has historically been discarded in deep-sea areas and underutilized. Improper dumping of dredged sediment will directly cause environmental pollution, especially harm to the diversity and richness of the benthic community [1]. In recent years, China has become the world's largest dredging country, with an annual dredging volume exceeding one billion cubic meters. The technology of UDS resource utilization is to process UDS into artificial blocks by a series of physical and chemical means to create more economical and ecological benefits in practical engineering. Meanwhile, with the increasing scarcity of sand and gravel resources, coupled with the implementation of policies prohibiting open-pit mining, UDS emerges as a promising substitute for construction materials.

Portland cement is the most widely used material in construction. Against this backdrop, some studies have confirmed that silicate concrete prepared with dredged sediments can improve performance, which fully demonstrates the great potential of dredged sand as building materials. Hassoune et al. [2] studied the feasibility of using dredged sand from the port of Agadir in concrete formulations. Their later research showed that the formulation based on dredged sand could be applied to construct a quay wall, which

was later proved stable [3]. Vafaei et al. [4] developed a high-strength concrete using seawater and dredged sea sand. They found that the dredged sea sand in concrete led to a considerable reduction in water absorption and sorptivity, which was consistent with what Limeira et al. [5] had previously discovered. Loudini et al. [6] evaluated the short-term and long-term mechanical behaviors of the silicate concrete based on dredged sediments, and the formulation worked out could be used in road foundation construction. However, dredged sediments from different rivers vary significantly in texture and characteristics. This mainly depends on the geological structure of the river, hydrological conditions, discharge, and sediment content. For example, mountainous rivers are often washed by rain, so the dredged sand particles are mostly stone sand, coarse particles with good mechanical strength and anti-erosion performance. In contrast, the UDS samples studied in this paper are from the plain area of the lower reaches of the Yangtze River. Due to the different hydrological conditions, the UDS has a finer texture and extremely small particles. The particles have a fineness modulus of 0.1–0.5 and a particle size of 0.075–0.3 mm. The particle surface of UDS is smooth, and there are problems such as irregular particles, much clay and lightweight. It is difficult for UDS to fully combine with Portland cement, resulting in mortar segregation. In the preliminary test, it was observed that the slurry containing UDS, which was directly solidified using Portland cement, exhibited poor quality and unstable strength in later stages. We have to explore other ways to utilize the UDS resources.

Geopolymer, a synthetic material formed by the reaction of aluminosilicate sources with alkaline hydroxide or silicate solutions, is a new environment-friendly material that can replace Portland cement [7,8]. Geopolymer has the advantages of fire resistance, high early strength, chemical corrosion resistance, and excellent durability, which brings broad application prospects in high-strength materials [7,9]. The construction industry faces the challenges of depleting fossil fuel reserves, scarcity of raw materials, increasing demand, growing environmental problems and a stagnant world economy. It is worth mentioning that producing 1 ton of Portland cement emits over 1 ton of CO_2, including both direct chemical reaction emissions and additional emissions from fuel combustion [10]. The cement industry is responsible for about 5–7% of the world's CO_2 emissions in the current scenario. The use of low-carbon geopolymer as a substitute for ordinary cement in solidifying dredged sand and further processing it into protective bricks, load-bearing blocks, and other artificial structures in the fields of ports and water conservancy can effectively solve the problems of dredged sand accumulation and landfilling, and realize the high value-added utilization of waste dredged sand. At the same time, the effective use of geopolymer reduces the amount of cement used, and thereby reduces the carbon emissions and energy consumption in the production and transportation of cement.

Some researchers have investigated the solidification of dredged materials with geopolymer. Anbarasan et al. [11] used dredged marine sand as a suitable replacement for the scarce river sand in geopolymer concrete production due to its corrosion resistance, resistance to carbonation, and alkalinity properties. Slimanou et al. [12] used metakaolin to solidify the dredged sediment waste of Bejaia port, and the highest compressive strength was 22 MPa when the content of calcined dredged sediment was 15 wt%. Lirer et al. [13] combined dredged sand with fly ash to prepare a geopolymer matrix with certain mechanical properties. The microstructure of the composite based on dredged sand was denser than that of ordinary siliceous sand. Hosseini et al. [14] used mechanochemical treatment of dredged clay to prepare a geopolymer mortar where inert clay can replace 50% of precursor mass. Zhang et al. [15] used fly ash-slag cementitious materials and recycled glass fiber reinforced plastic fibers to solidify dredged sludge, and it was observed that the post-rupture ductility of stabilized dredged sludge significantly increased with the increase in fiber content. The above studies indicate that geopolymer can be injected into dredged materials and form a three-dimensional network structure due to its high viscosity and adhesion properties. Upon contact with water, geopolymer rapidly absorbs water and swells, forming a gel that creates high-strength bonding and cohesive forces between dredged sand particles. These forces can effectively solidify the dredged sand and prevent it from settling

or slumping. Compared to Portland cement, geopolymer can solidify dredged sand and improve its mechanical performance and stability, which is not limited by the properties of the original dredged sand. Moreover, the alkali-activated system in geopolymer can easily produce significant drying shrinkage, which will cause non-uniform deformation and detrimental cracks [16–20]. UDS contains a significant amount of small particles and smooth surfaces, which can affect the bonding strength between geopolymer and sand particles, leading to reduced adhesive force, higher water absorption, and exacerbation of drying shrinkage. The harmful shrinkage cracks can create channels for various corrosive substances to penetrate the composite material, severely affecting the load-bearing capacity and durability [16].

Currently, potential fiber additives and the adjustment of alkali molar ratios are commonly used methods to enhance the mechanical performance and stability of geopolymer materials. However, for geopolymer-based solidification of UDS, the specific effects and optimal combinations of these factors, as well as their influence on the microstructure and shrinkage mechanism, have not been thoroughly investigated. In this study, by utilizing ground granulated blast-furnace slag (GGBS), UDS, sodium silicate (SS), and sodium hydroxide (SH), we developed a brand-new hybrid UDS-GGBS geopolymer (HUGG) paste. The experimental scheme was meticulously designed to clarify the influences of SS modulus and Na_2O content on the fluidity, setting time, mechanical properties, and shrinkage behavior of the HUGG paste. The microstructure was analyzed in detail by scanning electron microscope (SEM). Additionally, basalt and polypropylene fibers (BF and PPF) were employed to offset the linear drying shrinkage. This study aims to ensure that the HUGG concrete's mechanical properties and drying shrinkage conform to the engineering standards while simultaneously offering environmental and economic benefits. The blocks prepared from UDS should possess sufficient strength and the linear shrinkage rate during the drying process should be controlled within an acceptable range to avoid excessive stress. Fibers can be added to control cracks and prevent the expansion and damage caused by drying shrinkage. The HUGG paste utilizes abandoned UDS as raw material and transforms it into high-quality material suitable for concrete production. This reduces the demand for natural sand and preserves natural resources while also mitigating the carbon emissions associated with not using conventional cement, resulting in significant environmental benefits. The developed HUGG concrete can be a viable alternative to conventional concrete for producing small prefabricated units such as road paving blocks and interlocking pavers, which can be used in local applications for canal rehabilitation, road and municipal engineering projects.

2. Materials and Methods

2.1. Materials

2.1.1. UDS

The sand sample in this study came from the Ba Gua Zhou Branch Road Remediation Project in the Nanjing Reach of the Lower Yangtze River. The selected sand source area was located 10 m below the riverbed surface. Figure 1 shows the collection site of the UDS sample. The samples were analyzed by using a polarized light microscope. As shown in Figure 2, the UDS was transparent or translucent, with independent particles and no cohesion between particles. The predominant particle size distribution of the UDS falls within the range of 0.075 to 0.3 mm, as presented in Figure 3. The UDS sample has undergone thorough washing and drying, involving the following steps: mixing, sedimentation, separation, and drying. Firstly, the UDS is mixed with water and stirred to facilitate the separation of impurities and pollutants from the sand particles. After a certain period of stirring, the mixture is left undisturbed to allow sedimentation. During this process, heavier impurities and particles settle at the bottom of the mixture. The upper layer of clear water is then slowly poured out or separated using filtration methods to remove fine suspended impurities in the water. Finally, the washed UDS is placed in a suitable location for natural drying, and the natural morphology is shown in Figure 4a.

The mineral composition and physical characteristics of the UDS are shown in Table 1. The sand sample demonstrates a comparatively elevated concentration of SiO_2 and Al_2O_3.



Figure 1. The collection site of the UDS sample.

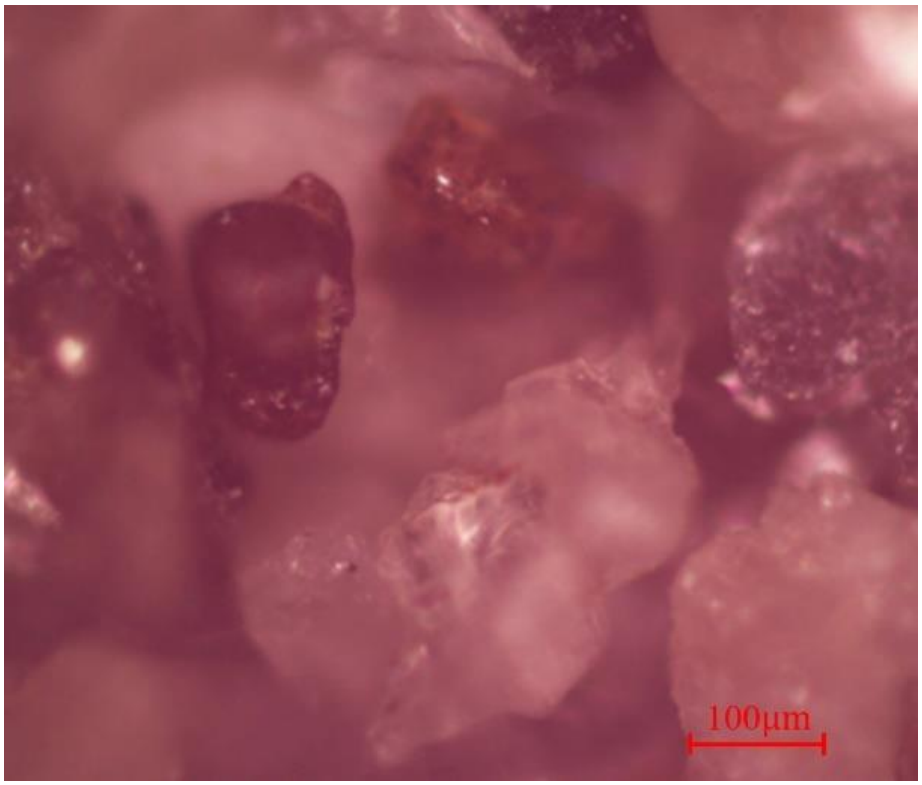


Figure 2. Polarizing microscope view of the UDS sample.

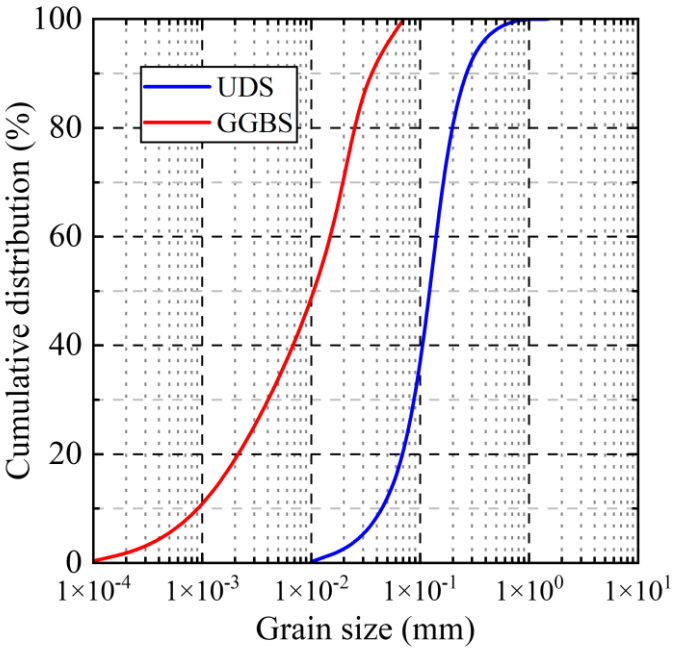
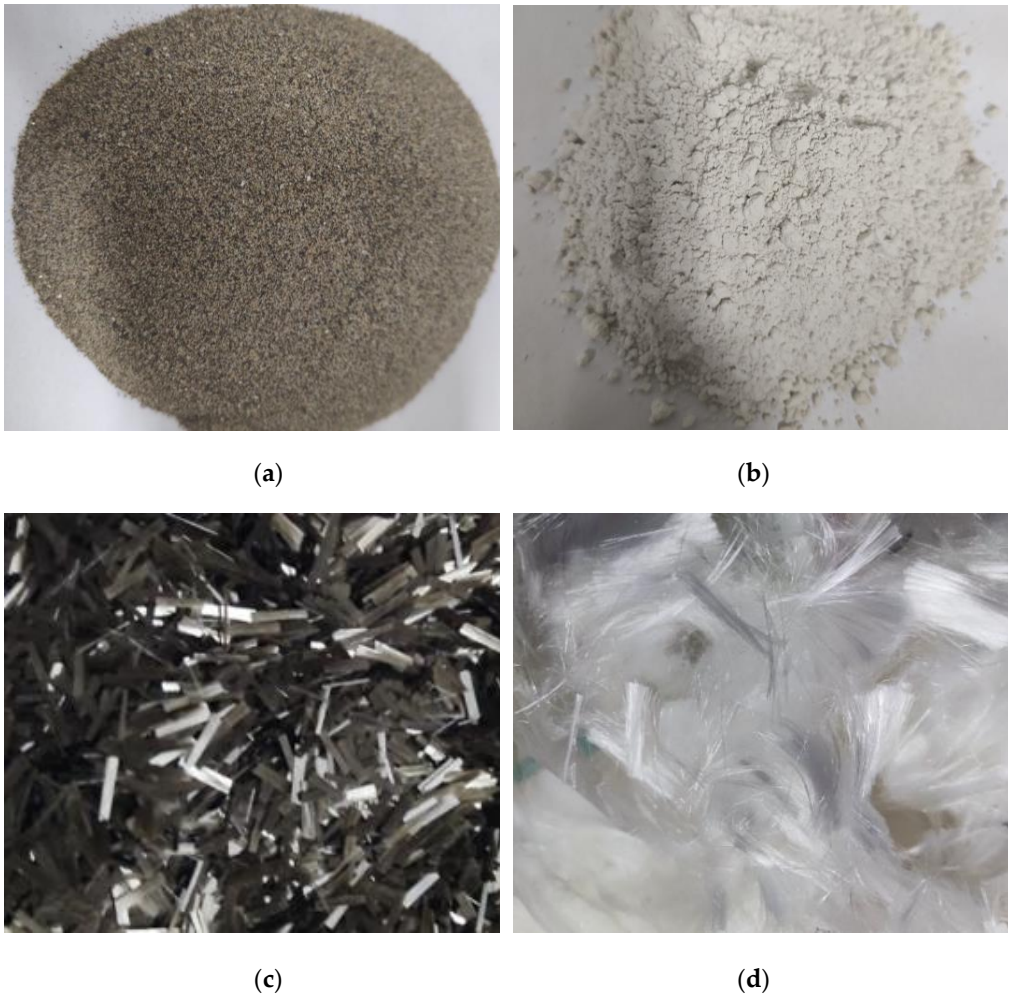


Figure 3. Size distributions of the studied UDS and GGBS.



(**a**) (**b**)

(**c**) (**d**)

Figure 4. The images of relevant materials needed for this study. (**a**) UDS; (**b**) GGBS; (**c**) BF; (**d**) PPF.

Table 1. The chemical compositions and the physical properties of UDS, GGBS, and SS.

Chemical Composition (wt%)	UDS	GGBS	SS
SiO_2	63.73	41.84	32.35
Al_2O_3	14.33	16.62	-
Fe_2O_3	4.82	0.46	-
CaO	8.54	36.74	-
MgO	3.42	3.16	-
K_2O	2.70	-	-
Na_2O	1.36	-	13.73
TiO_2	0.658	0.38	-
SO_3	0.04	-	-
Physical properties			
Specific surface (m^2/kg)	103	425	-
Density (g/cm^3)	2.62	2.8	1.53
Fineness modulus	0.1~0.5	-	-
Activity index (%)	-	>93	-
Modulus	-	-	2.43
Baume degree (Be)	-	-	50

2.1.2. GGBS

GGBS is a by-product of ironmaking, which can be acquired at approximately 1500 °C. GGBS-based geopolymer exhibits superior mechanical properties to Portland cement and other geopolymer materials [16]. In this study, GGBS was used as raw cementitious material, as shown in Figure 4b. The characteristics are given in Table 1.

2.1.3. Alkali-Activators

Previous studies have demonstrated that mechanical strengths of geopolymer composites are better when activated with sodium-based solutions than those activated with potassium-based or lithium-based solutions [10,21]. SS provides the element silicon, which can improve the crack resistance of geopolymer. This study employed a mixed alkali activator comprising SS and SH. SH, with a purity of 99.8%, is in the form of solid sheets, while SS is a translucent viscous liquid. Technical specifications of SS are provided in Table 1.

2.1.4. Chopped-Fibers

Two kinds of fibers, BF and PPF, have been used in this study, as shown in Figure 4c,d. The parameters of BF and PPF are given in Table 2.

Table 2. BF and PPF parameters.

Fiber Variety	Length (mm)	Density (g/cm^3)	Modulus of Elastic (GPa)	Tensile Strength (MPa)
BF	12	2.7	90	4100
PPF	12	0.91	6	600

2.1.5. Admixture

Geopolymer materials typically exhibit poor fluidity, and the incorporation of a high-efficiency water reducer can effectively decrease the viscosity of the slurry while maintaining its desired properties. This addition significantly enhances the flowability and workability of the concrete, facilitating easier placement and handling during construction processes. Ultra-fine dredged sand, known for its high water absorption characteristics, poses a challenge as increasing the water content can negatively impact the mechanical properties. Thus, the utilization of high-efficiency water reducers becomes essential to improve the compactness and strength of the slurry. According to Chinese national stan-

dard GB 8076-2008, this experiment used a polycarboxylate superplasticizer (SP) with a water-reducing rate of 25%.

2.2. Mix Design and Preparation of the Specimens

Before the commencement of the experimental program, a specified concentration of SH solution was prepared and allowed to cool for a duration of one hour. The mixed-activator solutions, possessing moduli of 0.5, 1.0, and 1.5, were subsequently prepared by combining the SH solution with SS. During the experiment, the mass percentage content of Na_2O in the composite activator was varied systematically to 3%, 4%, 5%, and 6% of the mass of GGBS, using precise calculation and weighing. The detailed specifications and parameters for each of these mix designs are presented in Table 3.

Table 3. Mix proportions of HUGG paste.

Mix ID	Na_2O Content	SS Modulus	Materials (kg/m^3)					
			UDS	GGBS	SS	SH	Additional Water	SP
C3-M0.5	3%	0.5	1132	566	25.5	17.5	269.2	4.53
C3-M1.0	3%	1.0	1132	566	50.7	12.9	255.6	4.53
C3-M1.5	3%	1.5	1132	566	75.5	8.5	242.2	4.53
C4-M0.5	4%	0.5	1132	566	33.9	23.2	264.7	4.53
C4-M1.0	4%	1.0	1132	566	67.5	17.2	246.6	4.53
C4-M1.5	4%	1.5	1132	566	100.7	11.3	228.7	4.53
C5-M0.5	5%	0.5	1132	566	42.5	29.1	260.1	4.53
C5-M1.0	5%	1.0	1132	566	84.2	21.5	237.5	4.53
C5-M1.5	5%	1.5	1132	566	125.6	14.2	215.3	4.53
C6-M0.5	6%	0.5	1132	566	50.9	34.9	255.5	4.53
C6-M1.0	6%	1.0	1132	566	101.3	25.8	228.3	4.53
C6-M1.5	6%	1.5	1132	566	150.9	17.0	201.5	4.53

GGBS, mixed-activator solution, water, and SP were first added into the cement paste mixer and stirred for 1.5 min. Subsequently, after the complete reaction of the geopolymer materials, UDS was incorporated and blended for another 1.5 min. The prepared HUGG paste was poured into standard test molds and vibrated for 2 min on a high-frequency shaking table. The relevant experimental instruments can be seen in Figure 5. Meanwhile, the slurry's surface was covered with a transparent film to prevent water loss. The optimal formulation was determined by conducting a series of tests to assess fluidity, setting time, and mechanical properties, based on the design scheme presented in Table 3. In the optimized experimental procedure, BF and PPF were utilized to compensate for drying shrinkage, corresponding to 0.1%, 0.2%, and 0.3% of the paste's volume fraction. The dredged sand and chopped fibers were pre-mixed before proceeding with the relevant steps described above. All specimens were maintained under constant conditions with a temperature of 25 °C and a humidity of 65%.

2.3. Testing Methods

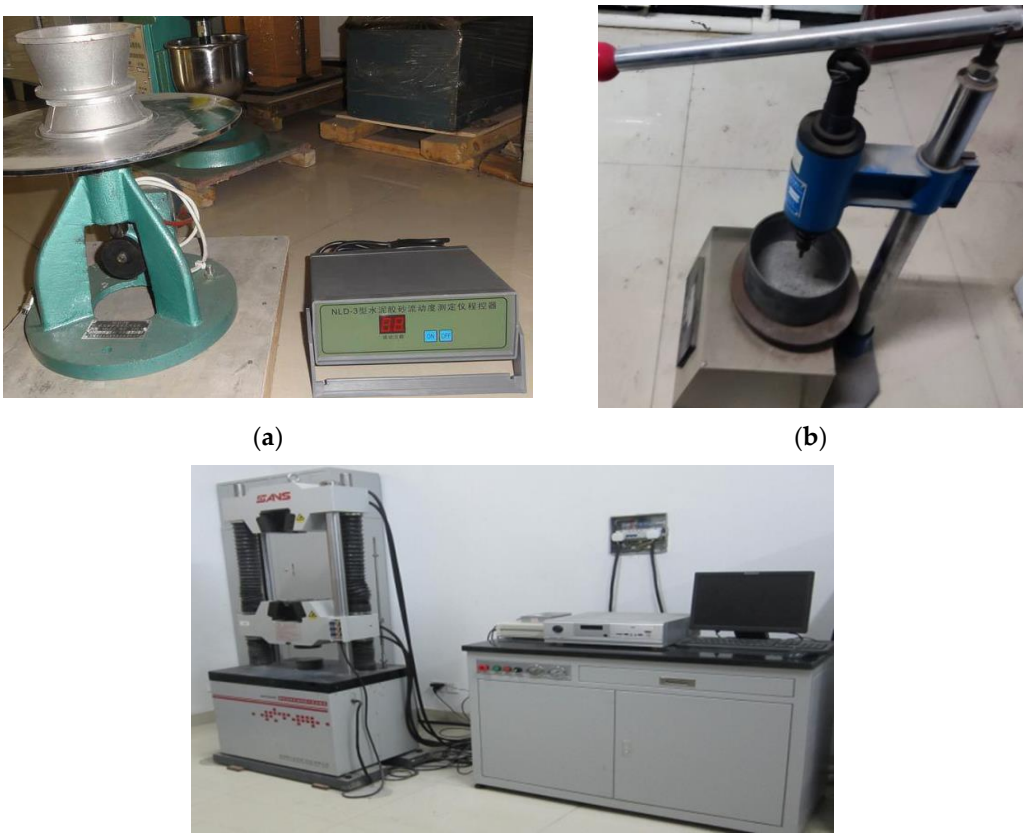
2.3.1. Fluidity

Fluidity tests were performed in agreement with GB/T2419-2005 standards. The testing equipment is shown in Figure 6a. The HUGG paste was poured into the fluidity test mold in two layers. The thickness of the first layer was about two-thirds of the height of the mold, and that of the second layer was 20 mm above the mold. The surface of the paste was scraped flat with a shovel knife after being vibrated evenly. Then, turning on the switch of the test platform aimed to perform 25 vertical drops at a rate of one per second. Finally, we measured the diameter of the two directions perpendicular to each other on the bottom surface of the paste with calipers, and the average value was calculated and taken as an integer.



(**a**) (**b**)

Figure 5. Instruments for making test blocks of concrete. (**a**) UJZ-15 cement paste mixer; (**b**) HZJ-A concrete shaking table.



(**a**) (**b**)

(**c**)

Figure 6. Measuring instruments for fluidity—NLD-3 cement mortar fluidity tester (**a**), setting time—Concrete penetration resistance meter (**b**), and mechanical properties—SHT4305 microcomputer controlled electro-hydraulic servo universal testing machine (**c**).

2.3.2. Setting Time

The setting time was tested in full compliance with SL/T 352-2020 specifications using a penetration resistance meter. Figure 6b shows the instrument used for the setting time tests. Unlike silicate concrete, geopolymer paste has a short initial setting time, which

leads to the need to shorten the early measurement interval and increase the test frequency. During the test, the end of the stylus was in contact with the surface of the mortar, and the stylus penetrated the mortar to a depth of 25 mm in 10 s. We measured two points on each mortar cylinder and took the average value. Measurements were made every 10 min starting from 15 min after the start of stirring the geopolymer materials with water. Taking time as abscissa and penetration resistance value as ordinate, the relation curve of penetration resistance value with time was drawn. Straight lines parallel to the abscissa were drawn at the penetration resistance values of 3.5 MPa and 28 MPa. The abscissas corresponding to the intersection points were the initial setting time and final setting time, respectively.

2.3.3. Compressive and Splitting Tensile Strength

According to SL/T352-2020, the compressive strength of UDS blocks was tested using the SHT4305 microcomputer-controlled electro-hydraulic servo universal testing machine. During the testing process, a continuously and uniformly applied load was exerted on the specimens that were cured to the specified age, with a loading rate of (0.3~0.5) MPa/s, until the specimens fractured. The failure load was recorded. The calculation formula for compressive strength of a cube is as follows:

$$f_{cc} = \frac{P}{A} \tag{1}$$

In the formula: f_{cc} represents the compressive strength (MPa); P represents the failure load (N); A represents the cross-sectional area of the specimen (mm^2).

The specimens were subjected to a test for splitting tensile strength. The specimens, cured to the specified age, were placed at the center of the compression plates. A parallel positioning line was drawn in the middle of the two side faces, and a pad was inserted between the upper and lower plates and the specimen, aligning it with the positioning line and oriented vertically. The loading speed was set to (1.8~3.6 MPa/min) until the specimen fractured, and the failure load was recorded. The formula for calculating the splitting tensile strength is as follows:

$$f_{ts} = \frac{2P}{\pi A} = 0.637\frac{P}{A} \tag{2}$$

In the formula: f_{ts} represents the splitting tensile strength (MPa); P represents the failure load (N); A represents the area of the split surface of the specimen (mm^2).

All measurements for the mechanical performance tests are taken three times. If a value differs from the median by more than 15%, the median value is adopted as the experimental result. If two values differ from the median by more than 15%, the entire set of results is considered invalid.

2.3.4. SEM

Representative samples cured for 28 days were selected and photographed by Hitachi SU8010 SEM for microstructure analysis.

2.3.5. Drying Shrinkage Compensation

The drying shrinkage test is based on SL/T352-2020. Similar methods have been reported before [22,23]. The BCII; vertical length comparator was used to measure the axial variation in shrinkage of samples at different ages. Figure 7 shows the illustration of the set-up for the drying shrinkage test. The displacement sensor of the electronic dial has a precision of 0.001 mm. The demolding time after one day was used as the starting point for

the drying shrinkage compensation test. The drying shrinkage value of a specimen at a certain age was calculated as follows:

$$\varepsilon_t = \frac{\Delta L_t}{L_1} = \frac{L_t - L_1}{L_1} \times 100 \quad (3)$$

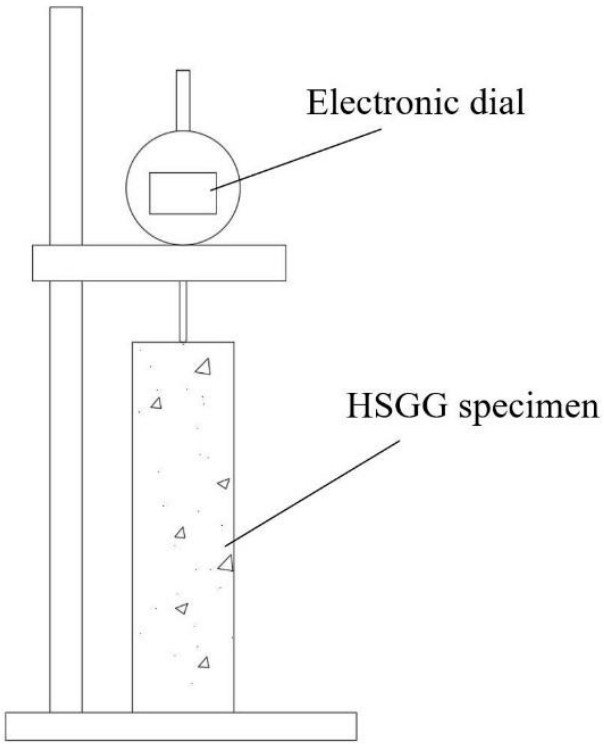


Figure 7. Illustration of the set-up for the drying shrinkage test.

In the formula: ε_t is the drying shrinkage value over the test time (mm/m); L_t is the linear measured length of the specimen on day t (mm); L_1 is the linear measured length of the specimen after the demolding on day 1 (mm).

3. Results and Discussion

3.1. Fluidity

The fluidity test results of HUGG pastes are presented in Figure 8. The fluidity of the slurry exhibits a reduction upon incrementing the Na_2O content and SS modulus. When the Na_2O content is 3%, the diffusion diameter of the slurry consistently exceeds 160 mm. With a content of 5%, the diffusion diameter is approximately 120 mm. However, when the Na_2O content increases from 5% to 6%, the diffusion diameter significantly decreases to around 80 mm, which severely impacts the operational performance of the slurry. The main reason is that the incremental alkali concentration in the reaction system accelerates the progress of the polycondensation reaction and quickly makes the slurry viscous. When the SS modulus increases, the high concentration of free silicon-oxygen (Si-O) tetrahedral groups promptly reacts with the dissolved calcium in GGBS to produce sufficient C-S-H gel, resulting in a drastic reduction in fluidity [24]. An excess of activation agent can accelerate the hydration reaction of geopolymer, resulting in the formation of a large amount of gelling substance and leading to a decrease in the fluidity of the concrete.

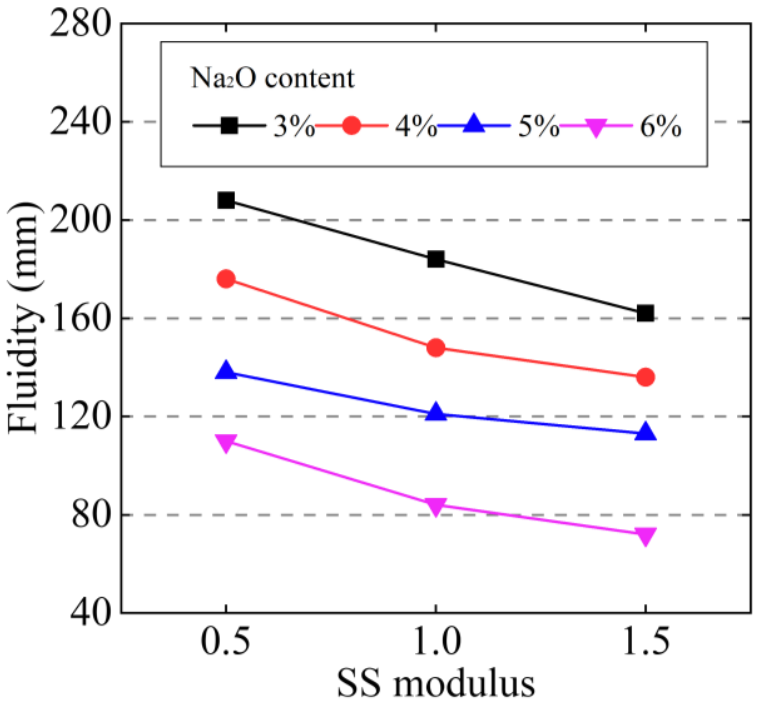


Figure 8. Influence of Na_2O content and SS modulus on the fluidity of HUGG paste.

The shape and size distribution of particles in UDS and GGBS have a significant influence on the fluidity of geopolymer. These raw materials typically contain small and irregular particles, leading to the development of cohesive and frictional forces that can reduce the fluidity of geopolymer. The presence of charges on the surface of particles in raw materials often leads to the formation of particle aggregates and precipitation through ion interactions, which can ultimately reduce the fluidity of the geopolymer. The fluidity and workability of fresh geopolymer paste are typically lower than those of conventional silicate concrete, owing to its inherent viscous and cohesive nature [25]. In this study, the HUGG paste can achieve compaction with vibrators even at low fluidity values.

3.2. Setting Time

Figure 9 shows the setting time test results of the HUGG pastes. The final setting times of different composition schemes are all less than 100 min. The slurry's initial and final setting times are negatively correlated with the Na_2O content and SS modulus. The increased alkali and soluble SiO_2 have accelerated the polymerization processes to a large extent. When the modulus is 1.0 and the Na_2O content is 5%, the initial and final setting time are 33 and 44 min, respectively. When the modulus is 1.0 and the Na_2O content is 6%, the initial and final setting time are 18 and 26 min, respectively. An increase in Na_2O content from 5% to 6% can result in a decrease of 45.46% and 40.9% in the initial and final setting time of the slurry, respectively. A flash-setting phenomenon was observed in the experimental group with a Na_2O content of 6%, as evidenced by the similarity of the initial and final setting times. Such a phenomenon is commonly associated with an excessively rapid hydration reaction rate, which can be attributed to inadequate mix design, subpar raw materials, or elevated Na_2O levels. Geopolymer's flash-setting can result in wasted resources and amplified production costs, as well as have detrimental effects on the mechanical properties of concrete structures, thereby posing a threat to the safety of construction projects.

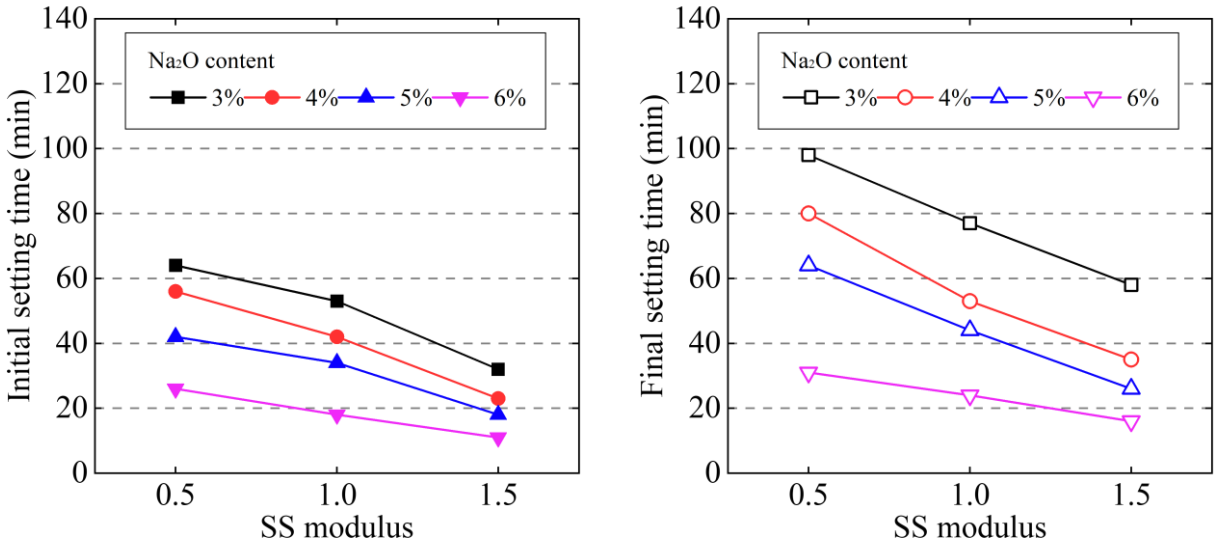


Figure 9. Influence of Na2O content and SS modulus on setting times of HUGG paste. (**a**) Initial setting time; (**b**) Final setting time.

The degree of condensation of geopolymer slurry can be related to the content of available calcium [10]. Free calcium ions dissolved from GGBS react with silicates to form C-S-H gel. C-S-H gel has a more open and porous structure that allows greater alkali/water diffusion through the gel, resulting in more gel formation and shorter setting time [10]. A sufficient amount of calcium can dramatically increase the early compressive strength of GGBS-based geopolymer but simultaneously reduce both the initial and final setting times [26]. The GGBS itself is more reactive, and its fine particles provide more reaction interfaces, increasing the contact area between the reactants and the solution, thereby accelerating the reaction rate. Before the geopolymer setting process begins, it is necessary to mix the mixture thoroughly to ensure consistent distribution of the UDS throughout the motor.

3.3. Influence of Na_2O Content on Mechanical Properties

The mechanical properties of different mix designs were examined at various test ages, and the results are presented in Figures 10 and 11. When the Na_2O content is below 4%, insufficient concentration of the activator can lead to a decrease in reaction rate, resulting in incomplete polymerization. This leads to an inadequate number and length of polymer chains, causing a reduction in cross-linking capability and subsequently lowering the strength of the geopolymer. A significant portion of the unreacted or partially reacted monomers may only serve as fillers or aggregates in the structure, contributing minimally to the overall strength of the geopolymer. It was found that Mix C5-M1.0 achieved the highest compressive and splitting tensile strengths of 56.53 MPa and 6.83 MPa, respectively, at 90 days. As the Na_2O content increased, both compressive and splitting tensile strengths generally increased with age. The compound SS-SH activator plays a dual role in alkali activation for preparing mortar. At a macroscopic level, the presence of Na_2O provides the necessary hydroxide environment for cementitious material reactions [17]. The degree of GGBS hydration is closely related to hydroxide concentration. Additionally, liquid SS provides various Si-O tetrahedral groups with different degrees of polymerization during the reaction. Adequate quantities of silicate and aluminate monomers are produced to facilitate the formation of a three-dimensional mesh with silicate and aluminate gel, thereby improving the mechanical properties [27].

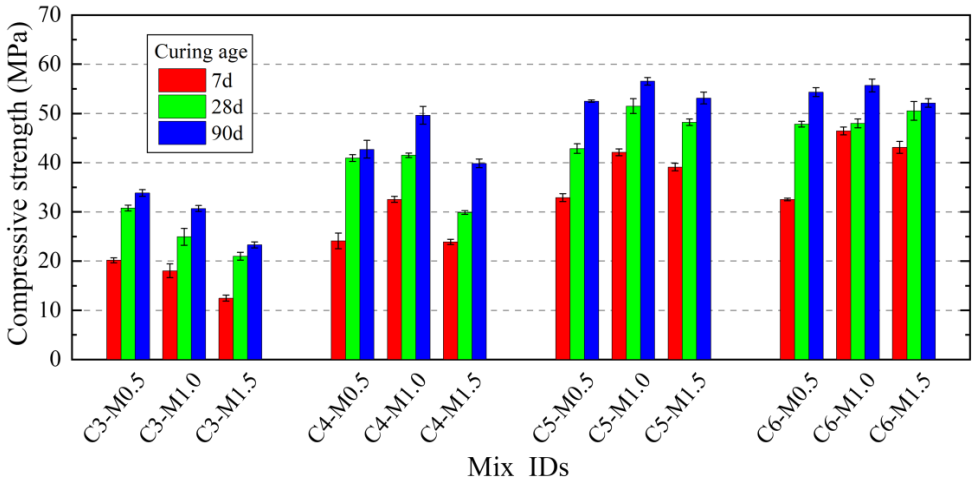


Figure 10. Influence of Na_2O content and SS modulus on the compressive strength of HUGG paste.

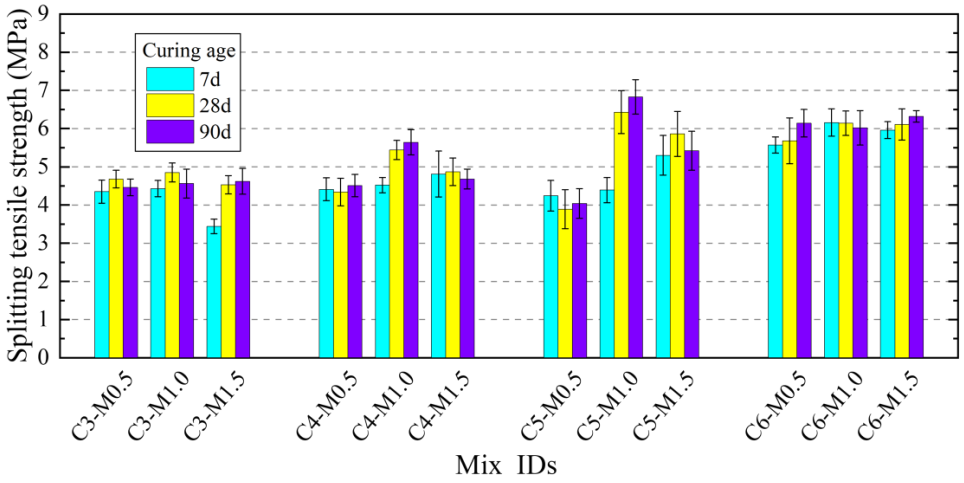


Figure 11. Influence of Na_2O content and SS modulus on the splitting tensile strength of HUGG paste.

However, it is important to note that increasing the concentration of alkali solutions does not always result in higher mechanical properties. For instance, when the SS modulus is kept constant at 1.0, and the Na_2O content increases from 5% to 6%, the compressive and splitting tensile strengths at seven days increase by 18.7% and 63.1%, respectively, while those at 90 days decrease by 8.5% and 11.9%, respectively. This is because an increased Na_2O content accelerates the hydrolysis and condensation hardening of the cementitious materials, leading to a significant decrease in setting time. During this flash-setting period, it was observed that some raw materials were only partially dissolved while the condensation hardening process had already occurred or even completed, thereby increasing the porosity and deteriorating the mechanical properties in the later stages.

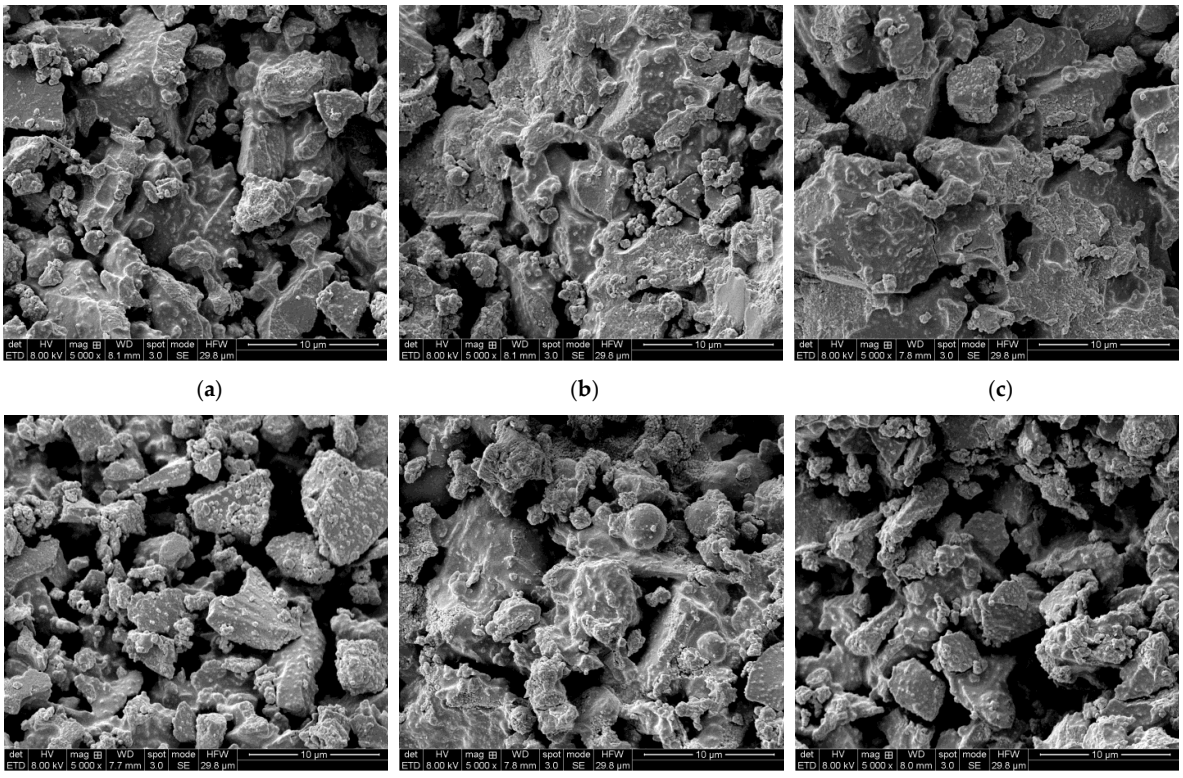
3.4. Influence of SS Modulus on Mechanical Properties

The compressive and splitting tensile strength of all mix designs almost reach their peak values when the SS modulus is 1.0. SS modulus has a greater influence on the splitting tensile strength of geopolymer compared to its compressive strength. When the Na_2O content is kept at 5%, an increase in modulus from 0.5 to 1.0 results in a 65.3% improvement in splitting tensile strength. Normally, an increased SS modulus provides more Si-O tetrahedral molecules with varying degrees of polymerization, which can facilitate the precipitation and polymerization of dissolved species [28]. Appropriate modulus can enhance the micro-network structure of geopolymer, providing it with higher splitting tensile strength.

When the Na_2O content is 4% or 5%, the compressive and splitting tensile strength with a modulus of 1.5 are lower than those with a modulus of 1.0. The high-modulus SS solutions often contain Si-O tetrahedral groups that are highly polymerized, leading to a propensity for self-polymerization, which in turn increases the solution's viscosity and diminishes its workability [7]. When high-modulus SS reacts with cementitious materials, it may generate sodium silicate gel containing sodium ions, which can cause cracks and looseness during the hardening process of geopolymers, ultimately reducing their mechanical properties and service life.

3.5. Microstructural Analysis

The HUGG specimens were subjected to SEM analysis to examine the particle morphology of hydration products after mechanical testing. The micrographs of the high-strength specimens at 28 days are presented in Figure 12. When the content of Na_2O is low, the geopolymer exhibits weaker gelation due to a lower degree of hardening, while with an increase, the gelation degree of geopolymer increases, leading to a denser gel network and improved mechanical properties. When the content of Na_2O is 5%, the formed geopolymer bonding structure is relatively dense (Figure 12a–c). The preparation of geopolymer is achieved through the reaction between aluminosilicate and alkaline activator. At the beginning of the reaction, hydroxide ions (OH^-) in the activator react with the metal-oxygen bonds in the aluminosilicate framework, forming Si-O and Al-O bonds. At this point, the pH value in the system gradually increases, accelerating the hydrolysis reaction and generating more Si-O and Al-O bonds, thereby increasing the network density of the polymer. When the network density of the polymer exceeds a certain limit, excessive polymerization occurs, resulting in the formation of a large number of cross-linking structures.



(**a**) (**b**) (**c**)

(**d**) (**e**) (**f**)

Figure 12. SEM images of HUGG samples at 28 days; high degree of polymerization and compact structure (**a**–**c**); the degree of polymerization decreases due to flash coagulation, and the interior is full of shrinkage cracks and pores (**d**–**f**). (**a**) C5-M0.5, (**b**) C5-M1.0, (**c**) C5-M1.5, (**d**) C6-M0.5, (**e**) C6-M1.0, (**f**) C6-M1.5.

Regarding the condensation process, the preparation of geopolymer requires a certain amount of time to allow for sufficient polymerization and the formation of a network structure. If the condensation time is insufficient, the polymer will exhibit incomplete polymerization. Flash-setting can cause a significant number of voids and cracks inside the geopolymer, and these defects can gradually expand during use, leading to instability and a shortened service life of the geopolymer. When Na_2O content increased from 5% to 6%, excessive Na_2O content can lead to flash-setting, causing the fracturing and looseness of the geopolymer matrix (Figure 12d–f). An excessive concentration of activator accelerates the progress of the polymerization reaction, leading to an increased rate of polymer chain formation during the curing process of geopolymer. This results in faster formation of the polymer network and cross-linking reactions, leading to greater shrinkage stress during the drying process. Moreover, a high concentration of activator can cause faster moisture loss from the geopolymer. Moisture plays a crucial role in the polymer curing process, and its evaporation and loss contribute to the volume shrinkage of the geopolymer. If the moisture loss rate is too rapid, the drying process will exhibit more pronounced shrinkage. In the case of UDS, the particles have a very small size, resulting in a high specific surface area. Due to the larger surface area, the polymer comes into contact with the surrounding environment more extensively, facilitating the evaporation of moisture. This accelerates the drying process of the polymer, leading to an intensified shrinkage phenomenon. The above reasons provide a detailed explanation for the formation of shrinkage cracks and pores within the matrix.

The presence of calcium in GGBS promotes the formation of amorphous C-S-H gel as the dominant hydration product when stimulated by SH and SS [29]. On the other hand, the reaction of aluminosilicate raw materials with high alkaline activators in geopolymers results in the dissolution and release of free $[SiO_4]^-$ and $[AlO_4]^-$ tetrahedral units, allowing the formation of a unique three-dimensional oxide network structure with Si-O-Al-O bonds [30]. Unlike Portland cement, which tends to produce weak interfacial adhesion with aggregate due to the enrichment of calcium hydroxide, geopolymer productions primarily form a three-dimensional network gel with covalent bonds that can closely combine with the aggregate to form a stable structure [7,31]. However, high concentrations of hydroxide may hinder the formation of C-S-H gel unless a substantial amount of calcium is provided, which can be effectively avoided by high-calcium GGBS in this study [29]. These cementitious matrices and stable structures formed by the hydration reaction products are crucial for the long-term development of mechanical properties.

By conducting comprehensive research on different formulations of the HUGG paste, we have explored their fluidity, setting time, mechanical strength, and microstructure. Our results indicate that the C5-M1.0 composition exhibits the most superior comprehensive performance among various formulations. The microstructure formed in this composition is highly dense, which endows the geopolymer with outstanding mechanical strength. Moreover, the C5-M1.0 composition can meet the requirements for fluidity and setting time in practical engineering applications, demonstrating high practicability and reliability.

3.6. Drying Shrinkage Compensation

Drying shrinkage, an inherent characteristic of cementitious materials, generally refers to the volume reduction in mortar under constant temperature curing [22]. In this study, samples with higher mechanical strengths are chosen for the drying shrinkage test, and the relationship between shrinkage values and curing ages is plotted in Figure 13. The test results show that the drying shrinkage value ranged from 0.65 mm/m to 1.10 mm/m. The drying shrinkage development of the HUGG paste can be categorized into three stages: acceleration (1–7 days), deceleration (7–21 days), and stabilization (21–90 days). The specimens with 5% Na_2O content exhibit lower contraction and better work performance. This is mainly due to the excessive alkali dosage in the activators when the Na_2O content increases to 6%, resulting in the slurry's quick-setting and the formation of capillary pores or cracks. Consequently, the specimens lose water continuously due to the imbalance

between the initial humidity of the material and the external environment, resulting in a significant increase in linear drying shrinkage value.

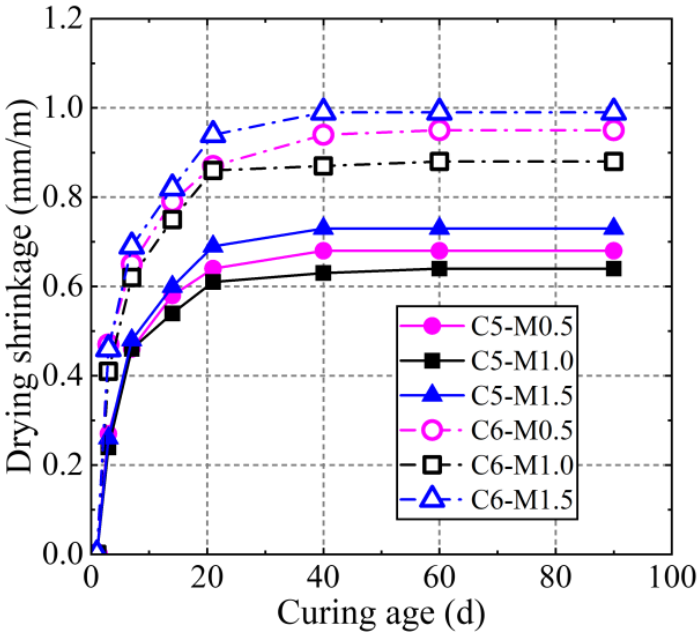


Figure 13. Variation in drying shrinkage values of HUGG paste with respect to Na_2O content and SS modulus.

To compensate for the drying shrinkage, BF and PPF were added to the mortar with varying proportions of 0.1%, 0.2%, and 0.3% of the mortar volume, using C5-M1.0 as the control group. The relevant test results are depicted in Figure 14. Table 4 shows the mechanical properties and 90-day density test outcomes. The control group exhibits a stable shrinkage value, which eventually reaches 0.65 mm/m. The addition of BF shows a direct proportionality with mechanical properties and 90-day density. In contrast, an increase in PPF content has a slightly positive effect on the early strength of the block, but it has a detrimental impact on the long-term development of compressive strength. The compressive strength decreases more seriously and even shrinks as the PPF content increases. The incorporation of PPF at levels of 0.2% and 0.3% can result in varying degrees of density reduction in the HUGG paste.

From Figure 14a, by adding 0.1%, 0.2%, and 0.3% of BF to the HUGG paste, the shrinkage values at 90 days were reduced to 0.54, 0.45, and 0.42 mm/m, respectively. BF mainly consists of SiO_2 and CaO as its main chemical components. The improved mechanical properties of HUGG paste are attributed to the increased calcium content in the system, which promotes the formation of additional C-S-H and C-A-S-H gel [32,33]. These additional products coexist with the N-A-S-H gel, resulting in the formation of a hybrid C-N-A-S-H gel [18]. Moreover, BF plays the micro aggregate role and increases the contact area between the UDS and GGBS in the reaction system due to good hydrophilicity. The three-dimensional disordered distribution of BF in the system can block the pores and transfer the stress, making the microstructure more compact and denser [30]. In summary, the unique structure and chemical properties of the surface of BF allow for interaction with geopolymer and UDS, thus forming a strong interfacial bond. This interfacial compatibility enhances the adhesive strength between geopolymer and UDS, increasing the synergistic effect between them and further reducing shrinkage. Previous studies have suggested that even a small amount of PPF (0.1% volume) can significantly improve the drying shrinkage of geopolymer concretes [18]. In our study, the addition of 0.1% PPF reduced the shrinkage value to 0.36 mm/m (Figure 14b). Two reasons may explain the deterioration of compressive strength. Firstly, the uneven dispersion of PPF in the system and excessive

fiber content can cause fiber agglomeration, leading to weak areas inside the block and ultimately reducing its compressive strength [18]. Secondly, the hydrophobic nature of PPF results in poor contact between substrates, leading to the entrainment of air and a decrease in compressive strength [34]. In an ordinary way, the tensile properties of concretes can be improved with appropriate additions of PPF [35]. This study shows a slight modification effect of PPF on the early splitting tensile strength. However, as the moisture evaporates in the later stages, the problematic contact between UDS and PPF deteriorates the pore structure, leading to little modification effect on the splitting tensile strength.

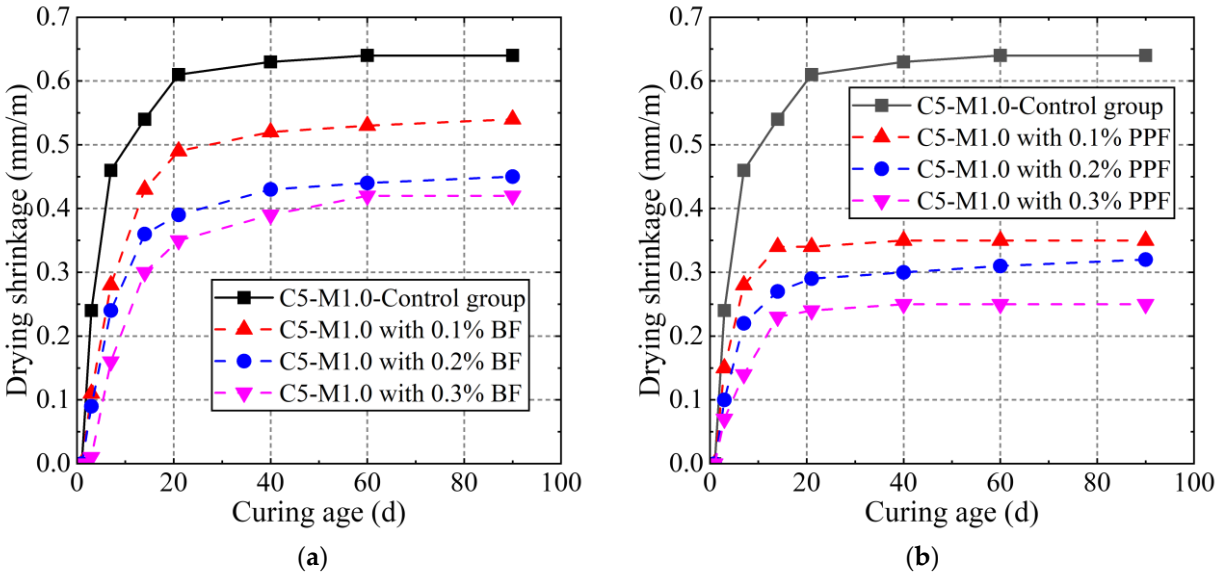


Figure 14. Effects of fiber incorporation on drying shrinkage of HUGG paste. (**a**) BF; (**b**) PPF.

Table 4. Mechanical properties and 90-day density test results of different fiber incorporation.

Mix IDs	Compressive Strength (MPa)			Splitting Tensile Strength (MPa)			90 d Density (kg/m^3)
	7 d	28 d	90 d	7 d	28 d	90 d	
C5-M1.0-Control group	39.11 (+0.00%)	48.20 (+0.00%)	56.53 (+0.00%)	4.39 (+0.00%)	6.43 (+0.00%)	6.83 (+0.00%)	2000.39 (+0.00%)
C5-M1.0 with 0.1%BF	42.28 (+8.12%)	51.94 (+7.75%)	61.17 (+8.21%)	4.78 (+8.94%)	6.46 (+0.50%)	7.05 (+3.23%)	2038.67 (+1.91%)
C5-M1.0 with 0.2%BF	44.52 (+13.82%)	55.31 (+14.75%)	62.10 (+9.85%)	5.36 (+22.05%)	6.78 (+5.49%)	7.75 (+13.41%)	2081.25 (+4.04%)
C5-M1.0 with 0.3%BF	50.76 (+29.79%)	56.06 (+16.32%)	61.73 (+9.20%)	5.84 (+32.99%)	7.47 (+16.24%)	8.58 (+25.06%)	2142.58 (+7.11%)
C5-M1.0 with 0.1%PPF	42.10 (+7.64%)	48.98 (+1.63%)	57.30 (+1.36%)	5.12 (+16.62%)	6.08 (−5.44%)	7.04 (+3.01%)	2006.25 (+0.29%)
C5-M1.0 with 0.2%PPF	39.26 (+0.39%)	42.28 (−12.27%)	41.09 (−27.31%)	5.60 (+27.63%)	6.35 (−1.24%)	6.80 (−0.43%)	1880.47 (−5.99%)
C5-M1.0 with 0.3%PPF	41.09 (+5.06%)	39.90 (−17.22%)	37.12 (−34.33%)	5.89 (+34.06%)	6.76 (+5.06%)	7.17 (+4.95%)	1860.16 (−7.01%)

In compliance with the GB/T 8239-2014 stipulations, masonry blocks are classified into two categories: L-type blocks for load-bearing structures and N-type blocks for non-load-bearing structures, based on the stress they undergo during use. The allowable maximum linear drying shrinkage value for L-type blocks is set at 0.45 mm/m, while for N-type blocks, it is 0.65 mm/m. Considering the toughening effect of different fibers and their dosages on HUGG pastes, the optimal fiber content of BF and PPF should be 0.2% and 0.1%, respectively, to satisfy the engineering requirements of L-type blocks. These optimal dosages were selected based on the experimental results, which indicate that these levels of fiber content can effectively compensate for the drying shrinkage of HUGG paste while maintaining adequate compressive and splitting tensile strength. It is worth

mentioning that BF is an eco-friendly, natural, and inexpensive inorganic fiber that has exceptional properties such as high strength, excellent stability, good chemical resistance, and high-temperature resistance. PPF, on the other hand, has shown little improvement in compressive strength and a slight improvement in early splitting tensile strength. This study recommends C5-M1.0 with 0.2%BF as the optimal solution, significantly impacting long-term mechanical performance development.

4. Conclusions

This study explored the influences of SS modulus and Na_2O content on the fresh properties and microstructure of HUGG paste made with UDS and GGBS. BF and PPF were used for drying shrinkage compensation in the optimal scheme. This study highlights the challenges of using UDS in geopolymer production due to its smooth surface, small particle size, and propensity for drying shrinkage. The main findings of the results can be concluded as follows:

(1) The fluidity and setting times of HUGG paste decrease with an increase in Na_2O content and SS modulus due to the acceleration of the polycondensation reaction. Fresh geopolymer paste has lower fluidity and workability than conventional silicate concrete, but HUGG paste can still be compacted with vibrators at low fluidity values. Flash-setting can occur with elevated 6% Na_2O content, which can lead to the loss of plasticity, decrease in strength, and reduction in durability.

(2) As the Na_2O content increases, there is a significant improvement in the mechanical properties of all specimens. The optimal Na_2O content of 5% is recommended to achieve maximum compressive strength and ensure the reliable performance of the slurry. Besides Na_2O content, the SS modulus is the second most influential factor affecting the mechanical properties of the HUGG paste. A suitable amount of Si-O tetrahedron groups can facilitate the polycondensation reaction of raw materials, while excessive polymerization can impede the depolymerization and polymerization processes of the material. At the maximum level, the HUGG concrete exhibits a compressive strength and splitting tensile strength of 56.53 MPa and 6.83 MPa, respectively, after 90 days of curing, with the optimal conditions of 5% Na_2O content and SS modulus of 1.0.

(3) SEM analysis of HUGG specimens showed that an increase in Na_2O content resulted in a denser gel network and improved mechanical properties. However, excessive Na_2O content can cause flash-setting, leading to the fracturing and looseness of the geopolymer matrix. The formation of voids and cracks due to incomplete polymerization can result in instability and a shortened service life of the geopolymer.

(4) The partial addition of BF can lower the shrinkage of HUGG pastes owing to its good hydrophilicity and also reinforce mechanical strengths. Considering the compensation effects and certain economic factors, 0.2% of the volume fraction of the paste is a suitable proportion. The 0.1% PPF can significantly inhibit the drying shrinkage, but the increasing volume percentage deteriorates the development of long-term mechanical properties.

This study shows that waste-dredged sand from the Yangtze River and GGBS-based geopolymer can be used to make artificial blocks that meet engineering requirements by adjusting alkali activators and adding fibers. As such, this approach presents a high value-added utilization approach for waste-dredged sand. This research holds significant potential for reducing the dependence on Portland cement, mitigating carbon emissions, and protecting the river environment.

HUGG is a complex material, and its performance is influenced by factors such as raw material composition, mix design, and preparation techniques. Due to variations in the source of materials, particularly the dredged sediments, conducting the same experiment in different laboratories or at different times may yield different results. Additionally, the experimental duration in this study was relatively short, which may not accurately simulate the long-term behavior of HUGG under sustained loading conditions. Therefore, the test

results might not capture the behavior of HUGG in the long term. While the impact of a single fiber on the contraction behavior of HUGG paste has been briefly explored, further investigation is necessary to comprehensively assess the long-term durability, corrosion resistance, and carbonization effects of mixed fibers when blended with HUGG paste. Future research on HUGG can focus on studying its long-term behavior, exploring the impact of different source materials, and conducting field-scale studies. These areas of investigation would provide valuable insights into the durability, performance, and real-world applicability of HUGG.

Author Contributions: Conceptualization, M.F. and C.J.; Investigation, M.F., Y.Z. and J.Z.; Data curation, Y.Z. and J.Z.; Formal analysis, Y.W., Y.Z. and J.Z.; Writing—review and editing, M.F. and C.J. All authors have read and agreed to the published version of the manuscript.

Funding: This research work is funded by the National Key Research and Development Program of China (2021YFB2600200), Key Research and Development Program of Guangxi (2021AB22114), and Postgraduate Research &Practice Innovation Program of Jiangsu Province (SJCX23_0191).

Data Availability Statement: All relevant data are within the paper.

Acknowledgments: The authors are deeply grateful to Hohai University for providing the experimental facilities and premises.

Conflicts of Interest: The authors declare no conflict of interest.

References

1. Fonseca, E.M.; Fernandes, J.R.; Lima, L.S.; Delgado, J.; Correa, T.R.; Costa, P.M.S.; Baptista Neto, J.A.; Aguiar, V.M.C. Effects of dredged sediment dumping on trace metals concentrations and macro benthic assemblage at the continental shelf adjacent to a tropical urbanized estuary. *Ocean. Coast. Manag.* **2020**, *196*, 105299. [CrossRef]
2. Hassoune, M.; Chraibi, G.; Fatmaoui, H.; Chaoufi, J. Requalification of dredging sediments through their use in concrete formulations based on a 3rd generation admixture. *Mater. Today Proc.* **2020**, *22*, 28–31. [CrossRef]
3. Hassoune, M.; Chraibi, G.; Fatmaoui, H.; Chaoufi, J. Stability of quay wall made on concrete blocks with a formulation based on dredging sand. *Mater. Today Proc.* **2021**, *36*, 47–53. [CrossRef]
4. Vafaei, D.; Hassanli, R.; Ma, X.; Duan, J.; Zhuge, Y. Sorptivity and mechanical properties of fiber-reinforced concrete made with seawater and dredged sea-sand. *Constr. Build. Mater.* **2021**, *270*, 121436. [CrossRef]
5. Limeira, J.; Etxeberria, M.; Agulló, L.; Molina, D. Mechanical and durability properties of concrete made with dredged marine sand. *Constr. Build. Mater.* **2011**, *25*, 4165–4174. [CrossRef]
6. Loudini, A.; Ibnoussina, M.; Witam, O.; Limam, A.; Turchanina, O. Valorisation of dredged marine sediments for use as road material. *Case Stud. Constr. Mater.* **2020**, *13*, e00455. [CrossRef]
7. Zhao, J.; Tong, L.; Li, B.; Chen, T.; Wang, C.; Yang, G.; Zheng, Y. Eco-friendly geopolymer materials: A review of performance improvement, potential application and sustainability assessment. *J. Cleaner Prod.* **2021**, *307*, 127085. [CrossRef]
8. Bianco, I.; Ap Dafydd Tomos, B.; Vinai, R. Analysis of the environmental impacts of alkali-activated concrete produced with waste glass-derived silicate activator–A LCA study. *J. Cleaner Prod.* **2021**, *316*, 128383. [CrossRef]
9. Cong, P.; Cheng, Y. Advances in geopolymer materials: A comprehensive review. *J. Traffic Transp. Eng.* **2021**, *8*, 283–314. [CrossRef]
10. John, S.K.; Nadir, Y.; Girija, K. Effect of source materials, additives on the mechanical properties and durability of fly ash and fly ash-slag geopolymer mortar: A review. *Constr. Build. Mater.* **2021**, *280*, 122443. [CrossRef]
11. Indhumathi Anbarasan, M.; Leema Margret, A.; Ragavan, V.; Ramprashath, J. Investigation on corrosion behaviour of geopolymer concrete using DMS and M−Sand as a fine aggregate under ambient curing conditions. *Mater. Today Proc.* **2023**, *in press*. [CrossRef]
12. Slimanou, H.; Bouguermouh, K.; Bouzidi, N. Synthesis of geopolymers based on dredged sediment in calcined and uncalcined states. *Mater. Lett.* **2019**, *251*, 188–191. [CrossRef]
13. Lirer, S.; Liguori, B.; Capasso, I.; Flora, A.; Caputo, D. Mechanical and chemical properties of composite materials made of dredged sediments in a fly-ash based geopolymer. *J. Environ. Manag.* **2017**, *191*, 1–7. [CrossRef]
14. Hosseini, S.; Brake, N.A.; Nikookar, M.; Günaydın-Şen, Ö.; Snyder, H.A. Enhanced strength and microstructure of dredged clay sediment-fly ash geopolymer by mechanochemical activation. *Constr. Build. Mater.* **2021**, *301*, 123948. [CrossRef]
15. Zhang, M.; Na, M.; Yang, Z.; Shi, Y.; Guerrieri, M.; Pan, Z. Study on mechanical properties and solidification mechanism of stabilized dredged materials with recycled GFRP fibre reinforced geopolymer. *Case Stud. Constr. Mater.* **2022**, *17*, e01187. [CrossRef]
16. Zhang, B.; Zhu, H.; Cheng, Y.; Huseien, G.F.; Shah, K.W. Shrinkage mechanisms and shrinkage-mitigating strategies of alkali-activated slag composites: A critical review. *Constr. Build. Mater.* **2022**, *318*, 125993. [CrossRef]

17. Mermerdaş, K.; Algın, Z.; Ekmen, Ş. Experimental assessment and optimization of mix parameters of fly ash-based lightweight geopolymer mortar with respect to shrinkage and strength. *J. Build. Eng.* **2020**, *31*, 101351. [CrossRef]
18. Farhan, K.Z.; Johari, M.A.M.; Demirboğa, R. Impact of fiber reinforcements on properties of geopolymer composites: A review. *J. Build. Eng.* **2021**, *44*, 102628. [CrossRef]
19. Nawaz, M.; Heitor, A.; Sivakumar, M. Geopolymers in construction-recent developments. *Constr. Build. Mater.* **2020**, *260*, 120472. [CrossRef]
20. Trincal, V.; Multon, S.; Benavent, V.; Lahalle, H.; Balsamo, B.; Caron, A.; Bucher, R.; Diaz Caselles, L.; Cyr, M. Shrinkage mitigation of metakaolin-based geopolymer activated by sodium silicate solution. *Cem. Concr. Res.* **2022**, *162*, 106993. [CrossRef]
21. Jegan, M.; Annadurai, R.; Kannan Rajkumar, P.R. A state of the art on effect of alkali activator, precursor, and fibers on properties of geopolymer composites. *Case Stud. Constr. Mater.* **2023**, *18*, e01891. [CrossRef]
22. Yuan, X.-h.; Chen, W.; Lu, Z.-a.; Chen, H. Shrinkage compensation of alkali-activated slag concrete and microstructural analysis. *Constr. Build. Mater.* **2014**, *66*, 422–428. [CrossRef]
23. Archez, J.; Farges, R.; Gharzouni, A.; Rossignol, S. Influence of the geopolymer formulation on the endogeneous shrinkage. *Constr. Build. Mater.* **2021**, *298*, 123813. [CrossRef]
24. Dehghani, A.; Aslani, F.; Ghaebi Panah, N. Effects of initial SiO2/Al2O3 molar ratio and slag on fly ash-based ambient cured geopolymer properties. *Constr. Build. Mater.* **2021**, *293*, 123527. [CrossRef]
25. Akhtar, N.; Ahmad, T.; Husain, D.; Majdi, A.; Alam, M.T.; Husain, N.; Wayal, A.K.S. Ecological footprint and economic assessment of conventional and geopolymer concrete for sustainable construction. *J. Cleaner Prod.* **2022**, *380*, 134910. [CrossRef]
26. Hanjitsuwan, S.; Hunpratub, S.; Thongbai, P.; Maensiri, S.; Sata, V.; Chindaprasirt, P. Effects of NaOH concentrations on physical and electrical properties of high calcium fly ash geopolymer paste. *Cem. Concr. Compos.* **2014**, *45*, 9–14. [CrossRef]
27. Luo, Y.; Jiang, Z.; Wang, D.; Lv, Y.; Gao, C.; Xue, G. Effects of alkaline activators on pore structure and mechanical properties of ultrafine metakaolin geopolymers cured at room temperature. *Constr. Build. Mater.* **2022**, *361*, 129678. [CrossRef]
28. Yong-Jie, H.; Cheng-Yong, H.; Yun-Ming, L.; Al Bakri Abdullah, M.M.; Yeng-Seng, L.; Ern-Hun, K.; Shee-Ween, O.; Wan-En, O.; Hui-Teng, N.; Yong-Sing, N. Strength optimization and key factors correlation of one-part fly ash/ladle furnace slag (FA/LFS) geopolymer using statistical approach. *J. Build. Eng.* **2023**, *63*, 105480. [CrossRef]
29. Ranjbar, N.; Kuenzel, C.; Spangenberg, J.; Mehrali, M. Hardening evolution of geopolymers from setting to equilibrium: A review. *Cem. Concr. Compos.* **2020**, *114*, 103729. [CrossRef]
30. Behera, P.; Baheti, V.; Militky, J.; Louda, P. Elevated temperature properties of basalt microfibril filled geopolymer composites. *Constr. Build. Mater.* **2018**, *163*, 850–860. [CrossRef]
31. Jiang, C.; Guo, W.; Chen, H.; Zhu, Y.; Jin, C. Effect of filler type and content on mechanical properties and microstructure of sand concrete made with superfine waste sand. *Constr. Build. Mater.* **2018**, *192*, 442–449. [CrossRef]
32. Punurai, W.; Kroehong, W.; Saptamongkol, A.; Chindaprasirt, P. Mechanical properties, microstructure and drying shrinkage of hybrid fly ash-basalt fiber geopolymer paste. *Constr. Build. Mater.* **2018**, *186*, 62–70. [CrossRef]
33. Xu, J.; Kang, A.; Wu, Z.; Xiao, P.; Gong, Y. Effect of high-calcium basalt fiber on the workability, mechanical properties and microstructure of slag-fly ash geopolymer grouting material. *Constr. Build. Mater.* **2021**, *302*, 124089. [CrossRef]
34. Qin, Y.; Li, Y.; Zhang, X.; Zhou, H. Constitutive model of polypropylene-fiber-fabric-reinforced concrete under uniaxial compression and index conversion of mechanical properties. *Constr. Build. Mater.* **2022**, *347*, 128508. [CrossRef]
35. Chen, X.; Zhou, M.; Shen, W.; Zhu, G.; Ge, X. Mechanical properties and microstructure of metakaolin-based geopolymer compound-modified by polyacrylic emulsion and polypropylene fibers. *Constr. Build. Mater.* **2018**, *190*, 680–690. [CrossRef]

Disclaimer/Publisher's Note: The statements, opinions and data contained in all publications are solely those of the individual author(s) and contributor(s) and not of MDPI and/or the editor(s). MDPI and/or the editor(s) disclaim responsibility for any injury to people or property resulting from any ideas, methods, instructions or products referred to in the content.